Received: 1 February 2024 | Revised: 3 May 2024 | Accepted: 8 May 2024

DOI: 10.1002/ardp.202400086

FULL PAPER

ARCH PHARM DPhG
Archiv der Pharmazie

Synthesis and in vitro cytotoxicity of benzoxazole-based PPARα/γ antagonists in colorectal cancer cell lines

Nazaret Moreno-Rodríguez[1] | Antonio Laghezza[2] | Carmen Cerchia[3] | Darina V. Sokolova[4,5] | Tatiana S. Spirina[4,5] | Barbara De Filippis[6] | Virgilio Romanelli[3] | Rocío Recio[1] | Inmaculada Fernández[1] | Fulvio Loiodice[2] | Vadim S. Pokrovsky[4,5] | Alessandra Ammazzalorso[6] | Antonio Lavecchia[3]

[1]Departamento de Química Orgánica y Farmacéutica, Facultad de Farmacia, Universidad de Sevilla, Sevilla, Spain

[2]Department of Pharmacy-Drug Science, University of Bari "Aldo Moro", Bari, Italy

[3]"Drug Discovery" Laboratory, Department of Pharmacy, University of Napoli "Federico II", Napoli, Italy

[4]Research, Institute of Experimental Therapy and Diagnostics of Tumor, NN Blokhin National Medical Center of Oncology, Moscow, Russia

[5]Department of Biochemistry, Patrice Lumumba Peoples' Friendship University, Moscow, Russia

[6]Department of Pharmacy, "G. d'Annunzio" University of Chieti-Pescara, Chieti, Italy

Correspondence

Alessandra Ammazzalorso, Department of Pharmacy, "G. d'Annunzio" University of Chieti-Pescara, Via Dei Vestini 31, 66100 Chieti, Italy.
Email: alessandra.ammazzalorso@unich.it

Antonio Lavecchia, Department of Pharmacy, "Drug Discovery" Laboratory, University of Napoli "Federico II", Via D. Montesano 49, 80131 Napoli, Italy.
Email: antonio.lavecchia@unina.it

Funding information

RUDN University Strategic Academic Leadership Program and State Project Ministry of Science and Higher Education of Russia, Grant/Award Number: agreement 075-01551-23-00; FSSF-2023-0006; PON R&I 2014-2020 Asse IV "Istruzione e Ricerca per il recupero - REACT-EU" and Azione IV.4 "Contratti di Ricerca su tematiche dell'Innovazione; FAR funds by Ministero dell'Istruzione, dell'Università e della Ricerca; Ministerio de Ciencia, Innovación y Universidades, Grant/Award Number: grant number PID2019-104767RB-I00; Italian Ministry of Education Progetti di Rilevante Interesse Nazionale, Grant/Award Number: 2022P5LPHS; European Regional Development Fund (ERDF) from FEDER; CITIUS

Abstract

A series of benzoxazole-based amides and sulfonamides were synthesized and evaluated for their human peroxisome proliferator-activated receptor (PPAR)α and PPARγ activity. All tested compounds showed a dual antagonist profile on both PPAR subtypes; based on transactivation results, seven compounds were selected to test their in vitro antiproliferative activity in a panel of eight cancer cell lines with different expression rates of PPARα and PPARγ. **3f** was identified as the most cytotoxic compound, with higher potency in the colorectal cancer cell lines HT-29 and HCT116. Compound **3f** induced a concentration-dependent activation of caspases and cell-cycle arrest in both colorectal cancer models. Docking experiments were also performed to shed light on the putative binding mode of this novel class of dual PPARα/γ antagonists.

KEYWORDS

amides, anticancer, benzoxazole, PPAR antagonists, sulfonamides

1 | INTRODUCTION

Since the discovery of peroxisome proliferator-activated receptors (PPARs), a lot of information was collected on these nuclear receptors, leading to the identification of three subtypes and a wide panel of biological actions. The cytotoxic potential of PPAR ligands has been attracting the attention and efforts of medicinal chemists, in the attempt to discover novel therapeutic options against cancer.[1–3] The PPARα subtype represents an interesting anticancer target, modulating the lipid catabolism and regulating the energetic pathways in proliferating cells.[4–6] In the last years, the possibility to obtain cytotoxic effects in cancer by PPARα antagonists has been widely assessed, with the discovery of several molecules potentially useful against different cancer types.[7–9] To date only preclinical data are available for these molecules, whereas a lead candidate recently entered clinical studies, with a very promising anticancer profile. TPST-1120 is a PPARα antagonist able to inhibit cancer cell proliferation by a dual mechanism of action, involving the lipid metabolism and the immune system. TPST-1120 has completed monotherapy dose escalation and a Phase 1/1b study in combination with nivolumab (NCT03829436). A randomized Phase 1b/2 study in combination with atezolizumab and bevacizumab in frontline patients with advanced hepatocellular carcinoma (HCC) is currently ongoing (NCT04524871) [Tempest Therapeutics website, https://www.tempesttx.com, accessed on January 5, 2024].

PPARγ has been widely investigated as the main target of thiazolidinediones (TZDs), which are used in type 2 diabetes mellitus and other diseases that feature insulin resistance.[10–12] However, due to crosstalk of signaling pathways, namely the regulation of PPARγ by phosphorylation through the MEK/ERK pathway, and the ability of PPARγ to form heterodimers with retinoid X receptors (RXRs), there is still some space for anticancer research of PPARγ as a target in cancer cells. PPARγ has been proven to be able to inhibit cell proliferation, induce cell-cycle termination and apoptosis, promote intercellular adhesion.[13,14] However, despite the multifunctional effects, the safety of PPARγ modulators is still of clinical concern.[15]

In the search for novel PPARα antagonists, our research group had previously identified some benzothiazole derivatives, endowed with antiproliferative activity in different cancer cell lines. Amide derivatives (structure a, Figure 1) displayed antiproliferative activities against pancreatic cell lines (AsPC-1, BxPC-3, Capan-2) and paraganglioma models (PTJ64i, PTJ86i)[16]; interestingly, they also showed a synergistic antiproliferative effect when tested in combination with gemcitabine on pancreatic cancer cells.[17] Acylsulfonamide derivatives (structure b, Figure 1) were discovered as PPARα antagonists, with IC_{50}s in the low micromolar range,[18] able to decrease cell viability in pancreatic (ASPC-1, Capan-2), colorectal (HT-29, SW480) cancer cell lines, and glioblastoma primary cells.

In this work, a novel series of compounds was designed, by replacing the benzothiazole nucleus with the benzoxazole, keeping the amide or sulfonamide functional groups (structures c and d, Figure 1), as compared with previously identified PPARα antagonists. The benzoxazole nucleus was unsubstituted (R = H) or decorated with a chlorine on C_5, whereas the aromatic ring linked to amide or sulfonamide moiety was differently substituted (X = H, Cl, F, NO_2). The replacement of the sulfur atom of the benzothiazole nucleus with the isosteric oxygen was suggested from the higher electronegativity of the latter, which could bring about higher polarity, greater potential of hydrogen bonding and, ultimately, a significant modification of the biological activity.

In the present investigation, we explored the potential of our benzoxazoles **3a–h** and **4a–g** against PPARα and PPARγ. Then, the cytotoxic activity of seven selected compounds was evaluated in vitro against a panel of cancer cell lines; the most cytotoxic compound **3f** was submitted to caspase activation assay and cell-cycle analysis, confirming an apoptotic effect in colorectal carcinoma cell lines HT-29 and HCT116.

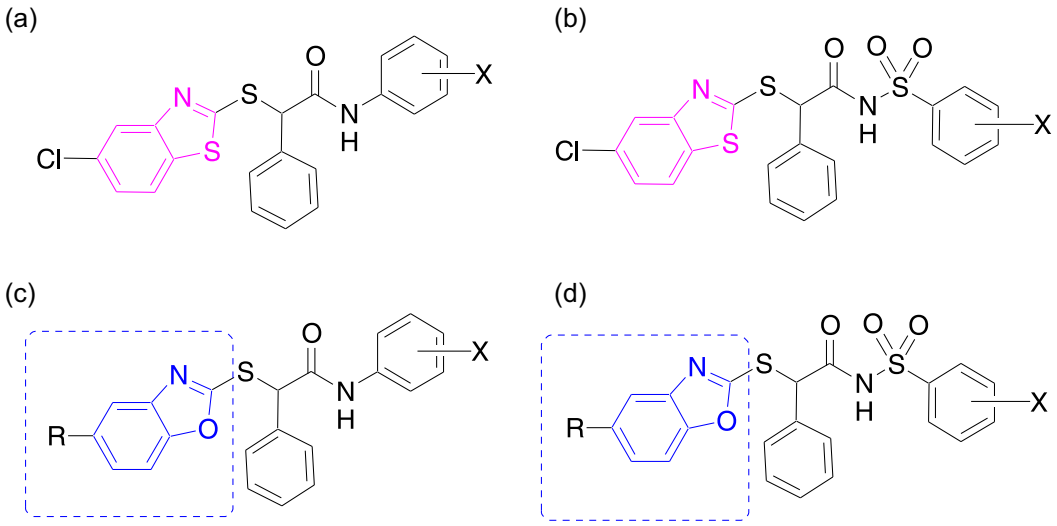

FIGURE 1 Antiproliferative benzothiazole derivatives (structures (a) and (b)) and novel amide and sulfonamide benzoxazole derivatives (structures (c) and (d)) synthesized in this work.

2 | RESULTS AND DISCUSSION

2.1 | Chemistry

Final compounds **3a–h** and **4a–g** were synthesized as reported in Scheme 1. The 2-mercaptobenzoxazole was reacted with ethyl α-bromophenylacetate, in THF and in the presence of triethylamine (TEA), from 0°C to room temperature for 21–23 h. In the ^{1}H-NMR spectra of the obtained esters, **1a–b**, it is worth noting the diastereotopic nature of the methylene protons in the ethyl group, appearing as two doublets of quartets. Esters **1a–b** were hydrolyzed by 2 N NaOH in THF, at room temperature, yielding carboxylic acids **2a–b**; they were then reacted with *N,N'*-dicyclohexylcarbodiimide (DCC), 1-hydroxybenzotriazole (HOBt), *N*-methylmorpholine (NMM) and the proper aniline in DMF to obtain amides **3a–h**, or with 1-ethyl-3-(3-dimethylaminopropyl)carbodiimide (EDC), 4-dimethylaminopyridine (DMAP) and the proper sulfonamide, in dry dichloromethane, under argon atmosphere, from 0°C to room temperature, to yield sulfonamide derivatives **4a–g**.

The structural elucidation and purity assessment of both amide (**3a–h**) and sulfonamide (**4a–g**) derivatives were accomplished via NMR spectroscopy (see the Supporting Information). Given their structural resemblance, both compound families exhibit a consistent pattern of characteristic signal shifts. In the ^{1}H-NMR spectra, a singlet attributed to the benzylic methine proton consistently appears shifted to the higher field (approximately 5.6 ppm). Additionally, in amides **3a–h**, a broad singlet corresponding to the NH moiety of the amide function is always observed shifted to the lower field (8.8–9.3 ppm). However, this distinctive signal cannot be observed in sulfonamides **4a–g** because spectra must be acquired in MeOD instead of $CDCl_3$, due to their insolubility. In the ^{13}C-NMR spectra, the signal of the benzylic carbon is likewise observed to be shielded in both derivatives, with resonances around 54 ppm in amides and in the range 57–59 ppm in sulfonamides. Furthermore, the carbonyl carbons exhibit deshielding effects, appearing at 166 ppm in amides and 176–171 ppm in sulfonamides, while the oxazole ring carbon can be observed in the range 164–166 ppm across all cases.

2.2 | Biology

2.2.1 | Evaluation of PPAR activity

First, the agonist activity of compounds **3a–h** and **4a–g** toward the human PPARα (hPPARα) and PPARγ (hPPARγ) subtypes was evaluated in vitro by a transactivation assay in which transiently transfected HepG2 cells were employed to express GAL4-PPAR chimeric receptors, according to a previously reported procedure.[19] Two concentrations (5 and 25 μM) were selected to evaluate the agonist activity of these compounds, which were compared with the corresponding reference agonists Wy-14,643 (EC_{50} on PPARα: 1.56 ± 0.30 μM) and rosiglitazone (EC_{50} on PPARγ: 0.039 ± 0.003 μM). Given that no significant activity

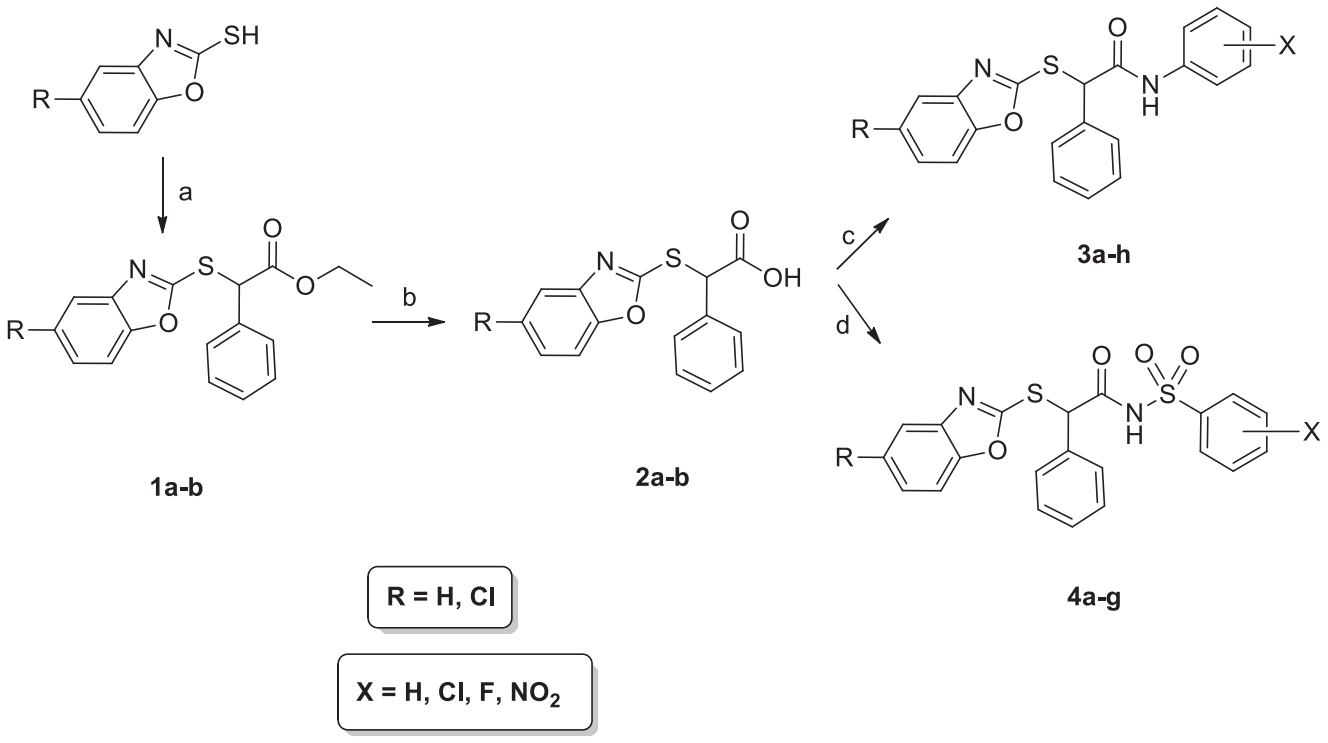

SCHEME 1 Synthesis of amides **3a–h** and sulfonamides **4a–g**. Reagents and conditions: (a) ethyl α-bromophenylacetate, TEA, THF, 0°C to rt, 21–23 h, 92%–98%; (b) 2 N NaOH, THF, rt, 17 h, quant; (c) DCC, HOBt, NMM, proper aniline, DMF, 0°C to rt, 20–23 h, 36%–60%; (d) EDC, DMAP, proper sulfonamide, dry dichloromethane, 0°C to rt, 22–23 h, 34%–80%.

was observed for all compounds (data not shown), we decided to investigate if they were endowed with some potential antagonist activity. For this purpose, we conducted a competitive binding assay in which PPARα and PPARγ activity in HepG2 cells was evaluated after co-treatment of a fixed concentration of the corresponding reference agonists Wy-14,643 (10 μM) and rosiglitazone (2 μM) and increasing concentrations of all compounds. As shown in Table 1, **3a–h** and **4a–g** displayed a moderate to good antagonist activity toward both receptor subtypes.

In the series of amides, derivatives substituted with the chlorine on the benzoxazole nucleus were slightly more potent than nonsubstituted analogs (**3e–h** vs. **3a–d**), with IC_{50s} in the range 7.9–21.0 μM on both PPAR subtypes. The substitution of benzene with chlorine or fluorine caused a weak decrease of potency, being the unsubstituted compound **3e** the most potent against both PPAR subtypes. Sulfonamides **4a–g** were more potent than corresponding amides, displaying IC_{50} values in the range of 2.6–18.2 μM. Among derivatives unsubstituted on the benzoxazole nucleus (**4a–c**), the introduction of a *p*-chloro substituent led to a better activity (**4c**, IC_{50} 4.68 and 2.6 μM on PPARα and PPARγ, respectively). A similar effect was observed in the chloro-substituted derivatives **4d–g**, all of them showing a similar potency on both subtypes, in the range of 2.7-5.3 μM. The introduction of a *m*-chloro substituent (**4f**) improved the potency, mainly on PPARα subtype (IC_{50} 2.71 μM).

The introduction of the benzoxazole, compared with the benzothiazole-based compounds previously synthesized by us, led to a dual α/γ antagonist profile, probably improving the binding within PPARγ binding pocket. In fact, benzothiazole compounds were found selective against PPARα.

2.2.2 | In vitro antiproliferative activity

Starting from transactivation assay results, seven compounds were selected to test their in vitro antiproliferative activity in a panel of cancer cells with different expression rate of PPARα and PPARγ (Supporting Information S1: Table S1). Compounds **3e** and **3f** were selected in the group of amides, displaying a similar antagonist behavior on both PPARα and PPARγ, whereas **4c–g** were selected as the most potent sulfonamide derivatives, showing IC_{50s} lower than 6 μM, in both PPAR subtypes. Eight cancer cell lines, representative of four cancer types (breast, colorectal, pancreatic, and lung cancer) were used in this study, performing the 3-(4,5-dimethylthiazol-2-yl)-2,5-diphenyltetrazolium bromide (MTT) assay. Dose–response curves for compounds against a panel of cancer cell lines are shown in Supporting Information S1: Figure S1. The calculated IC_{50} values, shown in Table 2, indicate **3f** as the most cytotoxic compound.

Overall tested compounds did not show remarkable cytotoxicity in the eight cancer cell lines; the most cytotoxic compound **3f** induced antiproliferative activity at concentrations ranging from 59.89 to 121.7 μM. Interestingly, the cytotoxic effect of **3f** was observed in most of the selected cancer cell lines, with the higher potency in colorectal cancer cells HT-29 and HCT116. To compare the selectivity of the cytotoxicity of **3f** between tumor and normal cells, the selectivity index (SI) was calculated by dividing the IC_{50} value for **3f** against human dermal fibroblasts (HDF) cells (culture of dermal fibroblasts) by the IC_{50} value of each colon cancer cell line. It was revealed that the SI for **3f** against normal human fibroblasts was higher than 3 in comparison with tumor cells (Supporting Information S1: Table S2). Based on the efficiency and selectivity of **3f**, we moved on to study the mechanism of death of the most sensitive human colon cancer cell lines.

The proapoptotic action of **3f** was evaluated using Muse® Caspase 3/7 Kit after 72 h co-incubation with **3f**. In HCT116 and HT29 cell lines, a dose-dependent caspases activation was observed (Figure 2, Supporting Information S1: Tables S3-4), reflecting the increased apoptosis after co-incubation. In the case of HCT116 cells, after co-incubation with **3f** at IC_{50} value, a statistically significant increase in the pool of both live and dead cells with activated effector caspases was observed: 55.2 ± 0.4% of live positive cells versus 34.8 ± 1.8% in control ($p < 0.001$) and 8.5 ± 1.0% of dead positive cells versus 2.5 ± 0.5% in control ($p = 0.001$), respectively. The total number of caspase-3/7 (+) cells dose-dependently increased compared with control at final concentrations of **3f** corresponding to its ½ IC_{50} and IC_{50}: 44.8 ± 0.4% ($p = 0.008$) and 63.7 ± 1.4% ($p < 0.001$) versus 37.3 ± 1.3% in control.

TABLE 1 hPPARα and hPPARγ antagonist activity by GAL-4 PPAR transactivation assay for compounds 3a–h and 4a–g.

	R	X	PPARαIC_{50} μM	PPARγIC_{50} μM		R	X	PPARαIC_{50} μM	PPARγIC_{50} μM
3a	H	H	23.1 ± 2.1	30.5 ± 5.6	**4a**	H	H	12.3 ± 1.87	8.08 ± 3.5
3b	H	*m*-F	26.8 ± 2.72	44.7 ± 2.6	**4b**	H	*p*-NO_2	18.2 ± 1.95	5.24 ± 1.35
3c	H	*m*-Cl	14.5 ± 1.9	52.0 ± 8.2	**4c**	H	*p*-Cl	4.68 ± 0.35	2.6 ± 0.4
3d	H	*p*-Cl	33.9 ± 5.8	27.2 ± 4.8	**4d**	Cl	H	4.56 ± 0.52	3.48 ± 0.34
3e	Cl	H	7.9 ± 1.13	12.2 ± 4.1	**4e**	Cl	*p*-NO_2	4.48 ± 1.95	5.19 ± 0.65
3f	Cl	*m*-F	9.79 ± 1.45	13.4 ± 1.76	**4f**	Cl	*m*-Cl	2.71 ± 0.07	3.9 ± 0.4
3g	Cl	*m*-Cl	13.11 ± 0.12	20.2 ± 4.4	**4g**	Cl	*p*-Cl	5.32 ± 0.15	3.7 ± 0.6
3h	Cl	*p*-Cl	13.5 ± 1.0	21.0 ± 2.3					

Abbreviation: PPAR, peroxisome proliferator-activated receptor.

TABLE 2 IC_{50} values of the selected compounds against human cancer cell lines.

	Cell lines, IC_{50}, μM[a]							
	SKBR3	A549	MDA-MB-231	HT-29	HCT 116	Capan-2	MCF-7	SW620
3e	>100	>100	>100	>100	>100	>100	>100	>100
3f	101.1 ± ND	97.89 ± ND	>100	59.89 ± 2.26	60.35 ± 5.39	85.82 ± 2.64	> 100	121.7 ± 33.4
4c	>100	>100	>100	>100	>100	>100	>100	>100
4d	>100	~100	>100	>100	~100	>100	>100	61.64±7.57
4e	>100	>100	>100	>100	~100	>100	>100	>100
4f	>100	>100	>100	>100	>100	>100	>100	>100
4g	>100	>100	>100	>100	~100	>100	>100	72.53 ± 10.53

Abbreviation: ND, not detected.

[a]Assays were performed in replicate ($n \geq 3$); IC_{50} values mean ± SD.

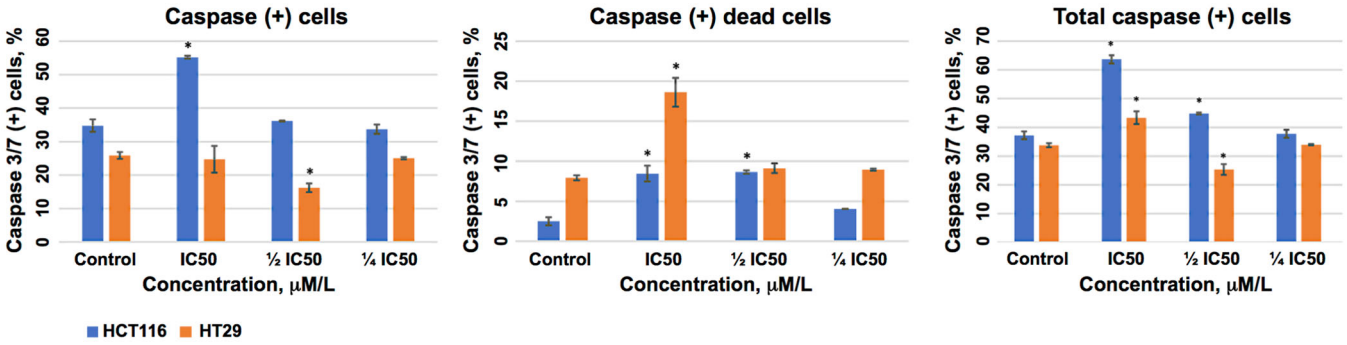

FIGURE 2 Dose-dependent activation of caspases by compound **3f** in HCT116 and HT29 cells after 72 h of co-incubation. The error bars represent ± SD.

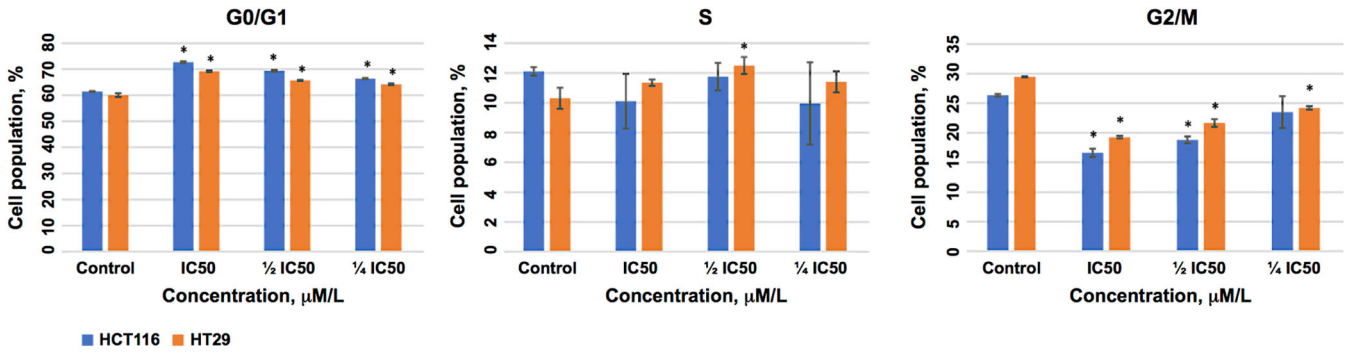

FIGURE 3 Compound **3f** induced cell-cycle arrest in HCT116 and HT29 cells after 72 h of co-incubation. The error bars represent ± SD.

In the case of HT29 cells, a statistically significant increase in the pool of (+) dead cells caspase-3/7 (2.4-fold compared with the control) was observed only after co-incubation with **3f** at IC_{50} value: 18.6 ± 1.8% versus 7.9 ± 0.3% in control ($p = 0.001$). At a concentration of **3f** corresponding to IC_{50}, an increase in the total number of cells with activated caspases 3/7 was also observed—43.4 ± 2.2% versus 33.8 ± 0.7 in control ($p = 0.007$).

Cell-cycle distribution after **3f** co-incubation with HCT116 and HT29 cells was evaluated using Muse® Cell Cycle Kit. The obtained results revealed that the compound induced a significant dose-dependent accumulation cells of both lines in the G0/G1 phase and a reduction of cells in G2/M (Figure 3, Supporting Information S1: Tables S5-6).

Comparable results were obtained through the utilization of three PPARγ inhibitors in assessing the impact on the survival of colorectal cancer (CRC) cells and a murine colorectal model.[20] The study revealed that lower doses (0.1–1 μM) of PPARγ inhibitors (T0070907, GW9662, and BADGE) exhibited no significant impact on cell survival.

In contrast, higher doses (10–100 μM) of all three PPARγ inhibitors induced caspase-dependent apoptosis in HT-29, Caco-2, and CRC LoVo cell lines. PPARγ inhibitors caused dual G and M cell-cycle arrest and microtubule loss through posttranscriptional regulation of tubulin.

Furthermore, our data align consistently with the findings presented in a study focused on evaluating the efficacy of a specific PPARα antagonist, GW6471, in advanced renal cell carcinoma.[21] The study demonstrated that PPARα antagonism affected the growth of 786-O and Caki-1 tumor cells through cell-cycle arrest in the G0/G1 phase and induction of apoptosis associated with a decrease in the levels of cell-cycle regulatory proteins CDK4, cyclin D1, and c-Myc. However, it is noteworthy that a similar proapoptotic effect and inhibition of cell proliferation were also revealed in the study of PPAR agonists. Thus, the report demonstrated the inhibition of HT29 culture growth due to the induction of apoptosis and cell-cycle arrest in the G0/G1 phase of the cell cycle after treatment of cells with PPARγ agonists rosiglitazone and 15-d-PGJ2.[22]

Additionally, intriguing data were obtained in another report,[23] showcasing that a synthesized series of chiral analogs of phenoxyacetic acid, functioning as partial PPAR agonists, induced cell-cycle arrest primarily through the activation of p21waf1/cip1. These analogs also antagonized the β-catenin/TCF pathway by inhibiting c-Myc and cyclin D1, suggesting their antiproliferative effect. Taken together, a detailed analysis of previous reports on the effects of newly synthesized compounds exhibiting agonist/antagonist activity against PPARs supports evidence for the pleiotropic function of these receptors in malignancy. These functions appear to depend on the type of cancer and/or the specific tumor microenvironment and require more detailed fundamental study.[24]

2.3 | Docking studies

To gain insights into the putative binding mode of these newly synthesized compounds, docking studies were performed using the Glide algorithm[25,26] and the X-ray crystal structures of PPARα in complex with the antagonist GW6471 (PDB ID: 1KKQ)[27] and PPARγ in complex with the antagonist SR11023 (PDB ID: 6C5T).[28] These structures were deemed appropriate for our studies because, in the case of PPARα, helix 12 (H12) features an inactive conformation due to the presence of the bound antagonist GW6471; in the case of PPARγ, the antagonist SR11023 provoked an allosteric switch in H12, which became fixed in an alternative location, able to prevent contacts with coactivator peptides and allowing binding of corepressor peptides (Supporting Information S1: Figure S2). The ligand binding domain (LBD) of PPARs is defined as "Y-shaped" and can be divided into a polar arm I, extending toward H12, a hydrophobic arm II, located between H3 and the β-sheet, and a hydrophobic entrance (arm III) (Supporting Information S1: Figure S2).

The binding mode of the most promising compound **3f**, showing antiproliferative activity and proapoptotic effects, is shown in Figure 4, whereas compounds **3e** and **4f** were also chosen for docking as potent, representative members of benzoxazole derivatives bearing amide (**3a–h**) and sulfonamide (**4a–g**) moieties, respectively. As the compounds under study feature a stereogenic carbon, both enantiomers were considered in docking calculations; the binding modes discussed below refer to the configuration of the selected pose for each compound, as detailed in Section 4 (Supporting Information).

Compound **3f** (*S* configuration) embraced H3 into PPARα LBD by forming a hydrogen bond with the carbonyl backbone of C276 through its amide group and several hydrophobic interactions, such as with F318, H440, F273 through the aromatic ring linked to amide which protruded in arm I; with V332 on the β-sheet, I272 and C276 on H3 through the benzoxazole moiety; with I317, L321 on H5, M330 on the β-sheet, through the unsubstituted phenyl ring (Figure 4a). The chlorine atom at position 5 of the benzoxazole contributed to filling the arm II pocket, and thus increasing potency toward this receptor subtype with respect to derivatives **3a–d** bearing the unsubstituted benzoxazole. The overlay of **3f** on the co-crystallized GW6471

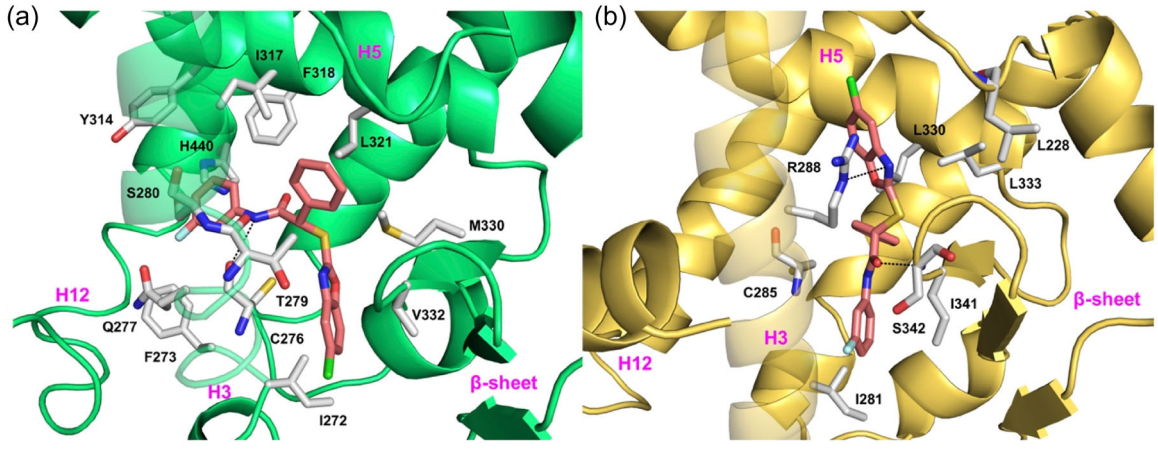

FIGURE 4 Binding mode of compound **3f** (deep salmon sticks) into peroxisome proliferator-activated receptor (PPAR)α (a) and PPARγ (b) ligand binding domains (LBDs), represented as green (PDB 1KKQ) and yellow (PDB 6C5T) ribbon models, respectively. Only amino acid residues discussed in the main text are displayed (white sticks) and labeled. H-bonds discussed in the text are depicted as dashed black lines.

showed a certain overlap of their phenyloxazole and benzoxazole rings, both extending toward arm II (Supporting Information S1: Figure S3).

The aromatic ring linked to amide might have a key role in determining an antagonist behavior of this series of ligands, with the smaller fluorine in *meta* position being preferred over chlorine (both in *meta* and *para*), likely because of possible steric clashes with H440. Notably, the most potent compound among derivatives **3a–h**, namely **3e**, has no substituents on such ring.

Compound **3f** displayed a slightly higher IC_{50} toward PPARγ (IC_{50} = 13.4 ± 1.76 μM); docking simulations suggested that the ligand fitted within H3 and the β-sheet, thereby accepting two H-bonds: one from the side chain of R288 on the nitrogen atom of the benzoxazole moiety, and a further one from the NH backbone of S342 on the carbonyl amide group (Figure 4b). The phenyl ring was encapsulated by hydrophobic interactions with L330 of helix H5 and C285 of helix H3, while the *m*-F phenyl group extended toward arm II. It is worth noting that switching from the benzothiazole to the benzoxazole nucleus allowed to gain antagonistic activity toward PPARγ. The benzoxazole is endowed with slightly higher polarity and likely greater potential of hydrogen bonding, which is key for engaging more strongly the polar residues within PPARγ, such as R288.

Compound **3e** (*S* configuration) overall maintained a similar binding mode to **3f** into PPARα LBD, with a minimal rearrangement due to the absence of substituents on the aromatic ring linked to the amide group. This latter formed two hydrogen bonds with the CO backbone of both C276 and T279 (Figure 5). Regarding PPARγ, compound **3e** (IC_{50} = 12.2 ± 4.1 μM) displayed a small improvement of the antagonistic activity but, overall, a very conserved binding mode was observed into the receptor (Figure 5). The presence of the chlorine atom at position 5 of the benzoxazole improved the activity, possibly because it is better packed within arm III pocket.

As regards **4f** (IC_{50} = 2.71 ± 0.07 μM), the representative most potent compound among derivatives **4a–g**, the sulfonamide moiety established a H-bond with the side chain of S280 into PPARα LBD (Figure 6), whereas the remainder of the ligand maintained overall the same hydrophobic interactions observed for **3f** and **3e** through the benzoxazole and phenyl rings (Figures 4 and 5). The role of substituents on the aromatic ring linked to sulfonamide was less clearly dissected, due to the higher rotational flexibility of sulfonamide; however, substitution in *meta* position was again preferred over *para* substitution.

Docking of **4f** into PPARγ LBD revealed that the highest ranked pose displayed *R* configuration and an opposite orientation with respect to **3f** and **3e**. **4f** was found to establish both an H-bond and a salt bridge with R288 through its sulfonamide group (Figure 6). The benzoxazole moiety of **4f** was also H-bonded to the S342 side chain. Finally, the *m*-Cl formed a halogen bond with L228. We observed that the chlorine substituent on the benzoxazole moiety was less relevant in the case of PPARγ, likely because it is rather solvent-exposed; in fact, **4c** showed the most potent activity among compounds **4a–g**. These latter turned out to be overall more active than their amide congeners, possibly because of the presence of the negatively charged sulfonamide moiety, which can more strongly interact with R288.

3 | CONCLUSIONS

Concluding, in this work a new series of PPAR antagonists was designed and synthesized by replacing the benzothiazole ring with a benzoxazole ring, while retaining the amide or sulfonamide functional groups. As hypothesized based on the different electronic properties of the oxygen atom, this replacement modified the biological activity of the obtained compounds, which demonstrated dual antagonistic behavior toward both PPARα and PPARγ. In vitro screening of the compounds led to the identification of lead **3f**, which demonstrated significant antiproliferative activity against a wide variety of human tumor cells. Our data show that **3f** induced apoptosis in the most

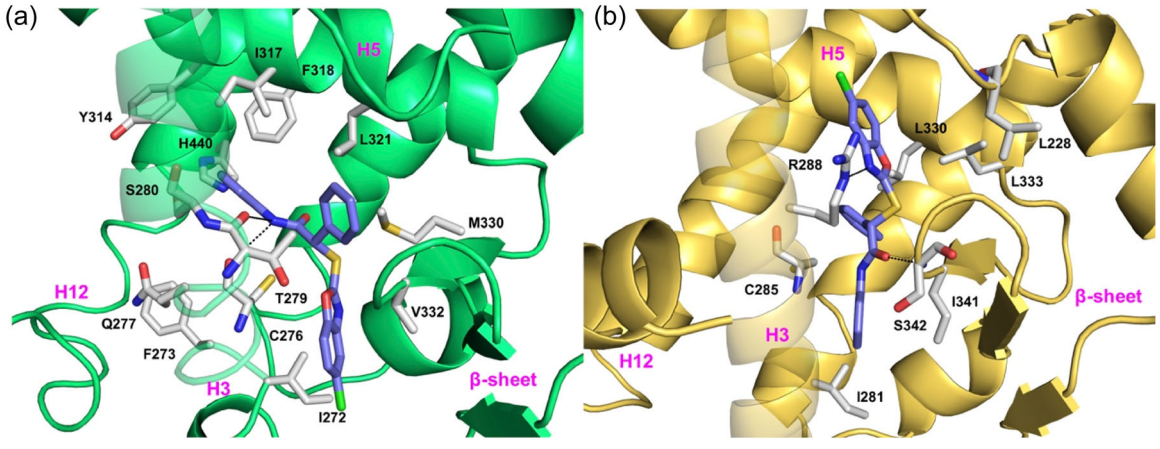

FIGURE 5 Binding mode of compound **3e** (slate sticks) into peroxisome proliferator-activated receptor (PPAR)α (a) and PPARγ (b) ligand binding domains (LBDs), represented as green (PDB 1KKQ) and yellow (PDB 6C5T) ribbon models, respectively. Only amino acid residues discussed in the main text are displayed (white sticks) and labeled. H-bonds discussed in the text are depicted as dashed black lines.

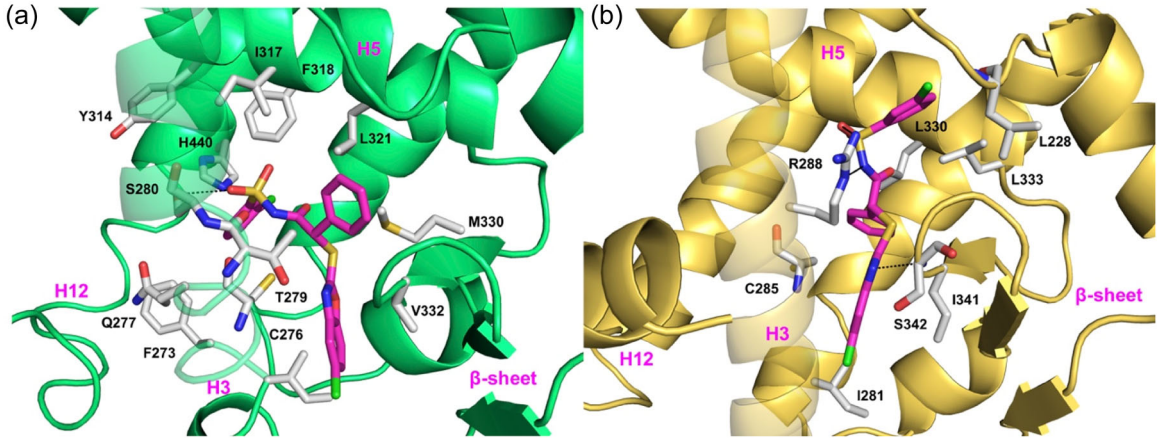

FIGURE 6 Binding mode of compound **4f** (magenta sticks) into peroxisome proliferator-activated receptor (PPAR)α (a) and PPARγ (b) ligand binding domain (LBDs), represented as green (PDB 1KKQ) and yellow (PDB 6C5T) ribbon models, respectively. Only amino acid residues discussed in the main text are displayed (white sticks) and labeled. H-bonds discussed in the text are depicted as dashed black lines.

sensitive colorectal cancer cell lines and triggered cell-cycle arrest. According to the Human Protein Atlas (www.proteinatlas.org), from the panel of culture lines selected for our study, colorectal cancer cells HCT116, HT29, and the pancreatic cancer line Capan-2 are characterized by a high level of expression of protein-coding genes PPARs, mainly PPARγ and to a lesser extent of PPARα expression (moderate level). This suggests that the dual antagonistic effect of **3f** on both PPARα and PPARγ likely accounts for the antiproliferative effects observed in these cells, although these findings require further studies. Moderate efficacy of pioglitazone in clinical trials in melanoma and HCC patients corroborates the hypothesis that PPARγ is an appropriate target on which further research efforts should be directed.[29,30]

It is not possible to exclude that, besides PPAR antagonism, other signaling pathways might be involved in the antiproliferative effects induced by **3f** in cancer cell lines. Based on current results, **3f** can be considered as a novel PPARα/γ dual antagonist deserving further investigation for its anticancer effects.

4 | EXPERIMENTAL

4.1 | Chemistry

4.1.1 | General

For the reactions which were run under an atmosphere of dry argon, oven-dried glassware and dried solvents were used. Chemicals were obtained from commercial sources and were used without further purification. TLC was carried out on silica gel GF254 (Merck), and compounds were detected by charring with phosphomolybdic acid/EtOH. For flash chromatography, Merck 230–400 mesh silica gel was used. Chromatographic columns were eluted with a positive pressure of air, and eluents are given as volume-to-volume ratios (v/v). NMR spectra were recorded with a Bruker Avance 500 MHz spectrometer. Chemical shifts are reported in ppm, and coupling constants are reported in Hz. Routine ^{1}H and ^{13}C spectra were referenced to the residual proton or carbon signals of the solvent, respectively. High-resolution mass spectra (HRMS) were recorded in the Centro de Investigación, Tecnología e Innovación in the University of Seville with a Kratos MS-80RFA 241-MC apparatus. Melting points were measured with a Stuart SMP3 apparatus in open-ended capillary tubes.

The InChI codes of the investigated compounds, together with some biological activity data, are provided as Supporting Information.

4.1.2 | General procedure for the synthesis of phenylacetic esters

To a solution of the corresponding 2-mercaptobenzo[*d*]oxazole (100 mol%) in THF at 0°C, Et_3N (200 mol%) was added. After 30 min, ethyl α-bromophenylacetate (100 mol%) was added dropwise at 0°C. After stirring overnight at room temperature, the solvent was evaporated under reduced pressure. Then CH_2Cl_2 (20 mL) and distilled water (20 mL) were added. The aqueous phase was extracted with CH_2Cl_2 (3 × 15 mL), and the combined organic phases were dried with anhydrous Na_2SO_4. The solvent was evaporated under reduced pressure and the reaction crude was purified by flash chromatography to obtain the desired compound.

Ethyl 2-(benzo[*d*]oxazol-2-ylthio)-2-phenylacetate (**1a**): Compound **1a** was prepared following the general procedure from benzo[*d*]oxazole-2-thiol (300 mg, 1.99 mmol), ethyl α-bromophenylacetate (348 µL, 1.99 mmol), Et_3N (553 µL, 3.98 mmol) and THF (17 mL). After 21 h, the resulting residue was purified by flash chromatography (cyclohexane/EtOAc, 6:1) to give **1a** (609.4 mg, 1.94 mmol, 98% yield) as a colorless liquid; ^{1}H NMR (500 MHz, $CDCl_3$): δ 7.56–7.54 (m, 1H), 7.51–7.49 (m, 2H), 7.34–7.37 (m, 1H), 7.35–7.28 (m, 3H), 7.23 (dt, J = 7.5 Hz, J = 1.2 Hz, 1H), 7.19 (dt, J = 7.5 Hz, J = 1.3 Hz, 1H), 5.64 (s, 1H), 4.25 (dq, J = 10.8 Hz, J = 7.1 Hz, 1H), 4.14 (dq, J = 10.8 Hz,

J = 7.1 Hz, 1H), 1.20 (t, J = 7.1 Hz, 3H) ppm; ^{13}C NMR (125 MHz, $CDCl_3$): δ 169.5, 163.1, 152.0, 141.9, 134.3, 129.2, 129.1, 128.6, 124.5, 124.3, 118.9, 110.1, 62.6, 54.0, 14.1 ppm; HRMS (ESI) *m/z*: $[M+Na]^+$ Calcd for $C_{17}H_{15}NNaO_3S$ 336.0665; found 336.0664.

Ethyl 2-[(5-chlorobenzo[*d*]oxazol-2-yl)thio]-2-phenylacetate (**1b**): Compound **1b** was prepared following the general procedure from 5-chlorobenzo[*d*]oxazole-2-thiol (300 mg, 1.62 mmol), ethyl α-bromophenylacetate (283 µL, 1.62 mmol), Et_3N (450 µL, 3.24 mmol), and THF (14 mL). After 23 h, the resulting residue was purified by flash chromatography (cyclohexane/EtOAc, 10:1) to give **1b** (518.1 mg, 1.49 mmol, 92% yield) as a yellow solid; mp 93–95°C; ^{1}H NMR (500 MHz, $CDCl_3$): δ 7.57 (d, J = 2.0 Hz, 1H), 7.55–7.53 (m, 2H), 7.40–7.33 (m, 4H), 7.21 (dd, J = 8.6 Hz, J = 2.1 Hz, 1H), 5.66 (s, 1H), 4.30 (dq, J = 10.8 Hz, J = 7.1 Hz, 1H), 4.19 (dq, J = 10.8 Hz, J = 7.1 Hz, 1H), 1.26 (t, J = 7.1 Hz, 3H) ppm; ^{13}C NMR (125 MHz, $CDCl_3$): δ 169.3, 164.9, 150.6, 143.0, 134.1, 130.1, 129.2 (2), 128.6, 124.4, 118.9, 110.8, 62.6, 54.1, 14.2 ppm; HRMS (ESI) *m/z*: $[M+Na]^+$ Calcd for $C_{17}H_{14}ClNNaO_3S$ 370.0275; found 370.0271.

4.1.3 | General procedure for the synthesis of phenylacetic acid derivatives

To a solution of the corresponding phenylacetic ester derivative (100 mol%) in THF, a 2 N NaOH aqueous solution (800 mol%) was added dropwise. After stirring overnight at room temperature, the solvent was evaporated under reduced pressure and the aqueous solution was acidified with an HCl 2 N solution to pH 1. Then, the aqueous layer was extracted with CH_2Cl_2 (3 × 15 mL), and the combined organic phases were washed with saturated aqueous NaCl solution (15 mL) and dried with anhydrous Na_2SO_4. The solvent was removed under vacuum to obtain the desired compound with no further purification.

2-(Benzo[*d*]oxazol-2-ylthio)-2-phenylacetic acid (**2a**): Compound **2a** was prepared following the general procedure from ethyl 2-(benzo[*d*]oxazol-2-ylthio)-2-phenylacetate **1a** (400 mg, 1.28 mmol), 2 N NaOH aqueous solution (5.1 mL, 10.21 mmol) and THF (4 mL). After 17 h, it was obtained **2a** (330 mg, 1.28 mmol, quant. yield) as an orange oil; ^{1}H NMR (500 MHz, $CDCl_3$): δ 7.55–7.54 (m, 1H), 7.50–7.48 (m, 2H), 7.39–7.38 (m, 1H), 7.35–7.31 (m, 3H), 7.25–7.19 (m, 2H), 5.62 (s, 1H) ppm; ^{13}C NMR (125 MHz, $CDCl_3$): δ 173.0, 163.5, 152.0, 141.3, 133.5, 129.4, 129.3, 128.7, 124.8, 124.6, 118.8, 110.3, 53.4 ppm; HRMS (ESI) *m/z*: $[M+Na]^+$ Calcd for $C_{15}H_{11}NNaO_3S$ 308.0352; found 308.0353.

2-[(5-Chlorobenzo[*d*]oxazol-2-yl)thio]-2-phenylacetic acid (**2b**): Compound **2b** was prepared following the general procedure from ethyl 2-[(5-chlorobenzo[*d*]oxazol-2-yl)thio]-2-phenylacetate **1b** (460 mg, 1.32 mmol), 2 N NaOH aqueous solution (5.3 mL, 10.6 mmol), and THF (4.5 mL). After 17 h, it was obtained **2b** (420 mg, 1.32 mmol, quant. yield) as an orange oil; ^{1}H NMR (500 MHz, $CDCl_3$): δ 7.58 (d, J = 2.0 Hz, 1H), 7.55–7.53 (m, 2H), 7.40–7.38 (m, 2H), 7.36–7.34 (m, 2H), 7.23 (dd, J = 8.6 Hz, J = 2.0 Hz, 1H), 5.66 (s, 1H) ppm; ^{13}C NMR (125 MHz, $CDCl_3$): δ 172.6, 165.0, 150.6, 142.5, 133.3, 130.3, 129.5, 129.4, 128.7, 124.8, 118.9, 110.9, 53.5 ppm; HRMS (ESI) *m/z*: $[M+Na]^+$ Calcd for $C_{15}H_{10}ClNNaO_3S$ 341.9962; found 341.9961.

4.1.4 | General procedure for the synthesis of amide derivatives

To a solution of the corresponding phenylacetic acid (100 mol%) in DMF at 0°C, HOBt (100 mol%) and DCC (100 mol%) were added. After stirring for 10 min, *N*-methylmorpholine (NMM) (100 mol%) and the corresponding amine (100 mol%) were added at 0°C. After stirring overnight at room temperature, the reaction was quenched with saturated aqueous $NaHCO_3$ solution (15 mL), and the aqueous phase was extracted with CH_2Cl_2 (3 × 15 mL). The combined organic phases were washed with saturated aqueous NaCl solution (15 mL) and dried with anhydrous Na_2SO_4. The solvent was evaporated under reduced pressure and the reaction crude was purified by flash chromatography to obtain the desired compound.

2-(Benzo[*d*]oxazol-2-ylthio)-*N*,2-diphenylacetamide (**3a**): Compound **3a** was prepared following the general procedure from 2-(benzo[*d*]oxazol-2-ylthio)-2-phenylacetic acid **2a** (184.1 mg, 0.65 mmol), HOBt (98.8 mg, 0.65 mmol), DCC (133.3 mg, 0.65 mmol), NMM (71 µL, 0.65 mmol), aniline (58.9 µL, 0.65 mmol), and DMF (3.8 mL). After 23 h, the resulting residue was purified by flash chromatography (cyclohexane/EtOAc, 4:1) to give **3a** (127.5 mg, 0.35 mmol, 55% yield) as a yellow solid; mp 138–140°C; ^{1}H NMR (500 MHz, $CDCl_3$): δ 9.02 (bs, 1H), 7.67 (d, J = 7.9 Hz, 1H), 7.59–7.58 (m, 2H), 7.53–7.50 (m, 2H), 7.47 (d, J = 8.0 Hz, 1H), 7.44–7.38 (m, 3H), 7.34 (dt, J = 7.6 Hz, J = 1.1 Hz, 1H), 7.31–7.27 (m, 3H), 7.09 (t, J = 7.4 Hz, 1H), 5.69 (s, 1H) ppm; ^{13}C NMR (125 MHz, $CDCl_3$): δ 166.8, 164.5, 152.2, 141.3, 137.9, 134.5, 129.3, 129.2 (2), 129.1, 128.9, 124.9, 124.7, 119.9, 118.5, 110.5, 54.4 ppm; HRMS (ESI) *m/z*: $[M+Na]^+$ Calcd for $C_{21}H_{16}N_2NaO_2S$ 383.0825; found 383.0821.

2-(Benzo[*d*]oxazol-2-ylthio)-*N*-(3-fluorophenyl)-2-phenylacetamide (**3b**): Compound **3b** was prepared following the general procedure from 2-(benzo[*d*]oxazol-2-ylthio)-2-phenylacetic acid **2a** (100 mg, 0.35 mmol), HOBt (54 mg, 0.35 mmol), DCC (72 mg, 0.35 mmol), NMM (38.5 µL, 0.35 mmol), 3-fluoroaniline (33.6 µL, 0.35 mmol) and DMF (2 mL). After 20 h, the resulting residue was purified by flash chromatography (cyclohexane/EtOAc, 5:1) to give **3b** (79.1 mg, 0.21 mmol, 60% yield) as a yellow solid; mp 149–151°C; ^{1}H NMR (500 MHz, $CDCl_3$): δ 9.38 (bs, 1H), 7.67 (d, J = 7.9 Hz, 1H), 7.57–7.56 (m, 2H), 7.50–7.47 (m, 2H), 7.44–7.38 (m, 3H), 7.35 (dt, J = 7.6 Hz, J = 1.0 Hz, 1H), 7.31 (dt, J = 7.7 Hz, J = 1.2 Hz, 1H), 7.22 (dt, J = 8.1 Hz, J = 6.4 Hz, 1H), 7.16–7.14 (m, 1H), 6.79 (dt, J = 8.2 Hz, J = 1.8 Hz, 1H), 5.66 (s, 1H) ppm; ^{13}C NMR (125 MHz, $CDCl_3$): δ 167.1, 164.7, 163.1 (d, $J_{C\text{-}F}$ = 244.9 Hz), 152.2, 141.1, 139.5 (d, $J_{C\text{-}F}$ = 10.7 Hz), 134.1, 130.2 (d, $J_{C\text{-}F}$ = 9.2 Hz), 129.2, 128.9, 125.0, 124.9, 118.4, 115.1 (d, $J_{C\text{-}F}$ = 2.82 Hz), 111.4 (d, $J_{C\text{-}F}$ = 20.8 Hz), 110.5, 107.5 (d, $J_{C\text{-}F}$ = 26.4 Hz), 54.1 ppm; HRMS (ESI) *m/z*: $[M+Na]^+$ Calcd for $C_{21}H_{15}FN_2NaO_2S$ 401.0730; found 401.0726.

2-(Benzo[*d*]oxazol-2-ylthio)-*N*-(3-chlorophenyl)-2-phenylacetamide (**3c**): Compound **3c** was prepared following the general procedure from 2-(benzo[*d*]oxazol-2-ylthio)-2-phenylacetic acid **2a** (150 mg, 0.53 mmol), HOBt (81 mg, 0.53 mmol), DCC (109 mg, 0.53 mmol), NMM (58 µL,

0.53 mmol), 3-chloroaniline (55 µL, 0.53 mmol) and DMF (3 mL). After 24 h, the resulting residue was purified by flash chromatography (hexane/EtOAc, 10:1) to give **3c** (108 mg, 0.27 mmol, 51% yield) as a white solid; mp 170–171°C; ^{1}H NMR (500 MHz, $CDCl_3$): δ 9.34 (bs, 1H), 7.69–7.66 (m, 2H), 7.57–7.56 (m, 2H), 7.48–7.47 (m, 1H), 7.44–7.38 (m, 3H), 7.37–7.29 (m, 3H), 7.19 (t, J = 8.1 Hz, 1H), 7.07–7.05 (m, 1H), 5.66 (s, 1H) ppm; ^{13}C NMR (125 MHz, $CDCl_3$): δ 167.1, 164.6, 152.2, 141.1, 139.1, 134.9, 134.1, 130.1, 129.2, 128.9, 125.0, 124.8, 124.7, 120.1, 118.5, 117.8, 110.5, 54.1 ppm; HRMS (ESI) *m/z*: $[M+Na]^+$ Calcd for $C_{21}H_{15}ClN_2NaO_2S$ 417.0435; found 417.0431.

2-(Benzo[*d*]oxazol-2-ylthio)-*N*-(4-chlorophenyl)-2-phenylacetamide (**3d**): Compound **3d** was prepared following the general procedure from 2-(benzo[*d*]oxazol-2-ylthio)-2-phenylacetic acid **2a** (150 mg, 0.53 mmol), HOBt (81 mg, 0.53 mmol), DCC (109 mg, 0.53 mmol), NMM (58 µL, 0.53 mmol), 4-chloroaniline (67.1 mg, 0.53 mmol) and DMF (3 mL). After 24 h, the resulting residue was purified by flash chromatography (hexane/EtOAc, 10:1) to give **3d** (116 mg, 0.29 mmol, 55% yield) as a white solid; mp 153–155°C; ^{1}H NMR (500 MHz, $CDCl_3$): δ 9.27 (bs, 1H), 7.67–7.65 (m, 1H), 7.57–7.56 (m, 2H), 7.48–7.46 (m, 3H), 7.43–7.38 (m, 3H), 7.35 (dt, J = 7.6 Hz, J = 1.2 Hz, 1H), 7.30 (dt, J = 7.7 Hz, J = 1.2 Hz, 1H), 7.25–7.23 (m, 2H), 5.66 (s, 1H) ppm; ^{13}C NMR (125 MHz, $CDCl_3$): δ 167.0, 164.6, 152.2, 141.1, 136.5, 134.2, 132.2, 129.7, 129.2 (2), 128.9, 125.0, 124.8, 121.2, 118.4, 110.5, 54.1 ppm; HRMS (ESI) *m/z*: $[M+Na]^+$ Calcd for $C_{21}H_{15}ClN_2NaO_2S$ 417.0435; found 417.0428.

2-[(5-Chlorobenzo[*d*]oxazol-2-yl)thio]-*N*,2-diphenylacetamide (**3e**): Compound **3e** was prepared following the general procedure from 2-[(5-chlorobenzo[*d*]oxazol-2-yl)thio]-2-phenylacetic acid **2b** (150 mg, 0.47 mmol), HOBt (72 mg, 0.47 mmol), DCC (97 mg, 0.47 mmol), NMM (51.6 µL, 0.47 mmol), aniline (42.8 µL, 0.47 mmol) and DMF (2.5 mL). After 21 h, the resulting residue was purified by flash chromatography (cyclohexane/EtOAc, 5:1) to give **3e** (65.8 mg, 0.17 mmol, 36% yield) as a yellow solid; mp 163–165°C; ^{1}H NMR (500 MHz, $CDCl_3$): δ 8.72 (bs, 1H), 7.62 (d, J = 2.0 Hz, 1H), 7.60–7.58 (m, 2H), 7.51–7.49 (m, 2H), 7.43–-7.36 (m, 4H), 7.32–7.28 (m, 2H), 7.26–7.24 (m, 1H), 7.11 (t, J = 7.4 Hz, 1H), 5.68 (s, 1H) ppm; ^{13}C NMR (125 MHz, $CDCl_3$): δ 166.6, 166.1, 150.7, 142.4, 137.7, 134.4, 130.4, 129.3 (2), 129.2, 128.9, 124.9 (2), 120.0, 118.6, 111.1, 54.9 ppm; HRMS (ESI) *m/z*: $[M+Na]^+$ Calcd for $C_{21}H_{15}ClN_2NaO_2S$ 417.0435; found 417.0431.

2-[(5-Chlorobenzo[*d*]oxazol-2-yl)thio]-*N*-(3-fluorophenyl)-2-phenylacetamide (**3f**): Compound **3f** was prepared following the general procedure from 2-[(5-chlorobenzo[*d*]oxazol-2-yl)thio]-2-phenylacetic acid **2b** (150 mg, 0.47 mmol), HOBt (72 mg, 0.47 mmol), DCC (97 mg, 0.47 mmol), NMM (51.6 µL, 0.47 mmol), 3-fluoroaniline (45 µL, 0.47 mmol) and DMF (2.5 mL). After 21 h, the resulting residue was purified by flash chromatography (cyclohexane/EtOAc, 4:1) to give **3f** (77.5 mg, 0.19 mmol, 40% yield) as a white solid; mp 185–186°C; ^{1}H NMR (500 MHz, $CDCl_3$): δ 8.94 (bs, 1H), 7.63 (d, J = 2.0 Hz, 1H), 7.57–7.56 (m, 2H), 7.44 (dt, J = 10.8 Hz, J = 1.9 Hz, 1H), 7.44–7.37 (m, 4H), 7.28 (d, J = 2.0 Hz, 1H), 7.24 (dt, J = 8.2 Hz, J = 6.4 Hz, 1H), 7.11 (dd, J = 8.1 Hz, J = 1.1 Hz, 1H), 6.80 (dt, J = 2.1 Hz, J = 8.2 Hz, 1H), 5.65 (s, 1H) ppm; ^{13}C NMR (125 MHz, $CDCl_3$): δ 166.8, 166.2, 163.1 (d, $J_{C\text{-}F}$ = 244.9 Hz), 150.7, 142.3, 139.2 (d, $J_{C\text{-}F}$ = 11.0 Hz), 134.0, 130.6, 130.3 (d, $J_{C\text{-}F}$ = 9.7 Hz), 129.4, 129.3, 128.9, 125.0, 118.6, 115.1 (d, $J_{C\text{-}F}$ = 2.8 Hz), 111.6 (d, $J_{C\text{-}F}$ = 21.3 Hz), 111.1, 107.5 (d, $J_{C\text{-}F}$ = 26.5 Hz), 54.6 ppm; HRMS (ESI) *m/z*: $[M+Na]^+$ Calcd for $C_{21}H_{14}ClFN_2NaO_2S$ 435.0341; found 435.0336.

2-[(5-Chlorobenzo[*d*]oxazol-2-yl)thio]-*N*-(3-chlorophenyl)-2-phenylacetamide (**3g**): Compound **3g** was prepared following the general procedure from 2-[(5-chlorobenzo[*d*]oxazol-2-yl)thio]-2-phenylacetic acid **2b** (200 mg, 0.63 mmol), HOBt (96 mg, 0.63 mmol), DCC (129 mg, 0.63 mmol), NMM (69 µL, 0.63 mmol), 3-chloroaniline (66 µL, 0.63 mmol), and DMF (4 mL). After 24 h, the resulting residue was purified by flash chromatography (hexane/EtOAc, 10:1) to give **3 g** (100.8 mg, 0.23 mmol, 37% yield) as a yellow solid; mp 152–154°C; ^{1}H NMR (500 MHz, $CDCl_3$): δ 8.87 (bs, 1H), 7.69–7.68 (m, 1H), 7.64 (d, J = 2.0 Hz, 1H), 7.57–7.56 (m, 2H), 7.44–7.38 (m, 4H), 7.31–7.27 (m, 2H), 7.22 (t, J = 8.1 Hz, 1H), 7.09–7.08 (m, 1H), 5.64 (s, 1H) ppm; ^{13}C NMR (125 MHz, $CDCl_3$): δ 166.8, 166.1, 150.7, 142.2, 138.8, 134.9, 134.0, 130.6, 130.1, 129.4, 129.3, 128.9, 125.0, 124.9, 120.2, 118.6, 117.9, 111.2, 54.7 ppm; HRMS (ESI) *m/z*: $[M+Na]^+$ Calcd for $C_{21}H_{14}Cl_2N_2NaO_2S$ 451.0045; found 451.0039.

2-[(5-Chlorobenzo[*d*]oxazol-2-yl)thio]-*N*-(4-chlorophenyl)-2-phenylacetamide (**3h**): Compound **3h** was prepared following the general procedure from 2-[(5-chlorobenzo[*d*]oxazol-2-yl)thio]-2-phenylacetic acid **2b** (131 mg, 0.41 mmol), HOBt (62.7 mg, 0.41 mmol), DCC (85 mg, 0.41 mmol), NMM (45 µL, 0.41 mmol), 4-chloroaniline (52.3 mg, 0.41 mmol), and DMF (2.5 mL). After 22 h, the resulting residue was purified by flash chromatography (hexane/EtOAc, 20:1) to give **3h** (99 mg, 0.23 mmol, 56% yield) as a yellow solid; mp 184–185°C; ^{1}H NMR (500 MHz, $CDCl_3$): δ 8.86 (bs, 1H), 7.62 (d, J = 2.0 Hz, 1H), 7.58–7.56 (m, 2H), 7.46–7.44 (m, 2H), 7.42–7.37 (m, 4H), 7.28–7.26 (m, 2H), 7.26–7.25 (m, 1H), 5.65 (s, 1H) ppm; ^{13}C NMR (125 MHz, $CDCl_3$): δ 166.7, 166.2, 150.7, 142.3, 136.3, 134.1, 130.5, 129.9, 129.4, 129.3, 129.2, 128.9, 125.0, 121.2, 118.5, 111.1, 54.6 ppm; HRMS (ESI) *m/z*: $[M+Na]^+$ Calcd for $C_{21}H_{14}Cl_2N_2NaO_2S$ 451.0045; found 451.0043.

4.1.5 | General procedure for the synthesis of sulfonamide derivatives

To a solution of the corresponding phenylacetic acid (100 mol%) under argon atmosphere in dry CH_2Cl_2 at 0°C, EDC (100 mol%), and DMAP (100 mol%) were added. After stirring during 10 min, the corresponding sulfonamide (100 mol%) were added at 0°C. After stirring overnight at room temperature, the reaction was quenched with distilled water (5 mL) and acidified with a 2 N HCl aqueous solution to pH 1, at 0°C. The aqueous phase was extracted with CH_2Cl_2 (3 × 15 mL). The combined organic phases were washed with saturated aqueous NaCl solution (15 mL) and dried with anhydrous Na_2SO_4. The solvent was evaporated under reduced pressure and the reaction crude was purified by flash chromatography to obtain the desired compound.

2-(Benzo[*d*]oxazol-2-ylthio)-2-phenyl-*N*-(phenylsulfonyl)acetamide (**4a**): Compound **4a** was prepared following the general procedure from 2-(benzo[*d*]oxazol-2-ylthio)-2-phenylacetic acid **2a** (150 mg, 0.53 mmol), EDC (101 mg, 0.53 mmol), DMAP (62 mg, 0.53 mmol), benzenesulfonamide (83 mg, 0.53 mmol), and CH_2Cl_2 (7.5 mL). After 23 h, the resulting residue was purified by flash chromatography (CH_2Cl_2/MeOH, 50:1) to give **4a** (158.2 mg, 0.37 mmol, 71% yield) as an orange solid; mp 169–170°C; ^{1}H NMR (500 MHz, MeOD): *δ* 7.82 (d, *J* = 7.4 Hz, 2H), 7.50–7.48 (m, 3H), 7.46–7.43 (m, 2H), 7.36–7.34 (m, 2H), 7.31–7.25 (m, 5H), 5.61 (s, 1H) ppm; ^{13}C NMR (125 MHz, MeOD): δ 174.6, 165.3, 153.0, 143.4, 142.7, 137.5, 133.1, 129.7 (2), 129.5, 129.4, 127.9, 125.6, 125.4, 119.3, 111.0, 58.7 ppm; HRMS (ESI) *m/z*: $[M+Na]^+$ Calcd for $C_{21}H_{16}N_2NaO_4S_2$ 447.0444; found 447.0439.

2-(Benzo[*d*]oxazol-2-ylthio)-*N*-[(4-nitrophenyl)sulfonyl]-2-phenylacetamide (**4b**): Compound **4b** was prepared following the general procedure from 2-(benzo[*d*]oxazol-2-ylthio)-2-phenylacetic acid **2a** (100 mg, 0.35 mmol), EDC (67 mg, 0.35 mmol), DMAP (43 mg, 0.35 mmol), 4-nitrobenzenesulfonamide (71 mg, 0.35 mmol), and CH_2Cl_2 (5 mL). After 22 h, the resulting residue was purified by flash chromatography (CH_2Cl_2/MeOH, 30:1) to give **4b** (108.7 mg, 0.23 mmol, 66% yield) as a yellow solid; mp 247–248°C; ^{1}H NMR (500 MHz, MeOD): δ 8.07 (d, *J* = 8.9 Hz, 2H), 7.93 (d, *J* = 8.9 Hz, 2H), 7.54–7.53 (m, 2H), 7.47–7.45 (m, 1H), 7.42–7.41 (m, 1H), 7.31–7.22 (m, 5H), 5.56 (s, 1H) ppm; ^{13}C NMR (125 MHz, MeOD): δ 176.7, 165.5, 152.8, 150.5 (2), 142.7, 138.2, 129.7, 129.6, 129.3, 129.1, 125.6, 125.4, 124.3, 119.2, 111.0, 59.4 ppm; HRMS (ESI) *m/z*: $[M+Na]^+$ Calcd for $C_{21}H_{15}N_3NaO_6S_2$ 492.0294; found 492.0290.

2-(Benzo[*d*]oxazol-2-ylthio)-*N*-[(4-chlorophenyl)sulfonyl]-2-phenylacetamide (**4c**): Compound **4c** was prepared following the general procedure from 2-(benzo[*d*]oxazol-2-ylthio)-2-phenylacetic acid **2a** (150 mg, 0.53 mmol), EDC (101 mg, 0.53 mmol), DMAP (62 mg, 0.53 mmol), 4-clorobenzenesulfonamide (101 mg, 0.53 mmol), and CH_2Cl_2 (7.5 mL). After 23 h, the resulting residue was purified by flash chromatography (CH_2Cl_2/MeOH, 50:1) to give **4c** (192.8 mg, 0.42 mmol, 80% yield) as an orange solid; mp 93–95°C; ^{1}H NMR (500 MHz, MeOD): *δ* 7.79 (d, *J* = 8.7 Hz, 2H), 7.50–7.48 (m, 2H), 7.46–7.41 (m, 2H), 7.33–7.26 (m, 7H), 5.60 (s, 1H) ppm; ^{13}C NMR (125 MHz, MeOD): δ 173.6, 165.0, 153.0, 142.6, 141.5, 139.5, 136.6, 129.9 (2), 129.8, 129.7, 125.7, 125.5, 119.3, 111.0, 58.1 ppm; HRMS (ESI) *m/z*: $[M+Na]^+$ Calcd for $C_{21}H_{15}ClN_2NaO_4S_2$ 481.0054; found 481.0048.

2-[(5-Chlorobenzo[*d*]oxazol-2-yl)thio]-2-phenyl-*N*-(phenylsulfonyl) acetamide (**4d**): Compound **4d** was prepared following the general procedure from 2-[(5-chlorobenzo[*d*]oxazol-2-yl)thio]-2-phenylacetic acid **2b** (100 mg, 0.31 mmol), EDC (60 mg, 0.31 mmol), DMAP (38 mg, 0.31 mmol), benzenesulfonamide (49 mg, 0.31 mmol), and CH_2Cl_2 (5 mL). After 23 h, the resulting residue was purified by flash chromatography (CH_2Cl_2/MeOH, 30:1) to give **4d** (86.8 mg, 0.19 mmol, 61% yield) as a yellow solid; mp 196–198°C; ^{1}H NMR (500 MHz, MeOD): δ 7.91 (d, *J* = 7.6 Hz, 2H), 7.56–7.52 (m, 1H), 7.43–7.41 (m, 6H), 7.36–7.35 (m, 3H), 7.28 (dd, *J* = 2.1 Hz, *J* = 8.5 Hz, 1H), 5.62 (s, 1H) ppm; ^{13}C NMR (125 MHz, MeOD): δ 171.0, 166.6, 151.7, 143.8, 141.5, 135.0, 134.2, 131.1, 130.2 (2), 129.7 (2), 128.7, 125.5, 119.4, 112.0, 56.9 ppm; HRMS (ESI) *m/z*: $[M+Na]^+$ Calcd for $C_{21}H_{15}ClN_2NaO_4S_2$ 481.0054; found 481.0047.

2-[(5-Chlorobenzo[*d*]oxazol-2-yl)thio]-*N*-[(4-nitrophenyl)sulfonyl]-2-phenylacetamide (**4e**): Compound **4e** was prepared following the general procedure from 2-[(5-chlorobenzo[*d*]oxazol-2-yl]thio)-2-phenylacetic acid **2b** (100 mg, 0.31 mmol), EDC (60 mg, 0.31 mmol), DMAP (38 mg, 0.31 mmol), 4-nitrobenzenesulfonamide (63 mg, 0.31 mmol), and CH_2Cl_2 (5 mL). After 23 h, the resulting residue was purified by flash chromatography (CH_2Cl_2/MeOH, 50:1) to give **4e** (106.2 mg, 0.21 mmol, 68% yield) as a yellow solid; mp 223–225°C; ^{1}H NMR (500 MHz, MeOD): δ 8.09 (d, *J* = 8.4 Hz, 2H), 7.94 (d, *J* = 8.7 Hz, 2H), 7.54–7.53 (m, 2H), 7.44–7.43 (m, 1H), 7.39–7.37 (m, 1H), 7.29–7.27 (m, 3H), 7.23–7.20 (m, 1H), 5.55 (s, 1H) ppm; ^{13}C NMR (125 MHz, MeOD): *δ* 176.6, 167.5, 151.5, 150.6, 144.0, 138.0, 131.1, 129.7, 129.6, 129.4, 129.0, 125.3, 124.4 (2), 119.1, 111.9, 59.5 ppm; HRMS (ESI) *m/z*: $[M+Na]^+$ Calcd for $C_{21}H_{14}ClN_3NaO_6S_2$ 525.9905; found 525.9899.

2-[(5-Chlorobenzo[d]oxazol-2-yl)thio]-*N*-[(3-chlorophenyl)sulfonyl]-2-phenylacetamide (**4f**): Compound **4f** was prepared following the general procedure from 2-[(5-chlorobenzo[*d*]oxazol-2-yl)thio]-2-phenylacetic acid **2b** (200 mg, 0.63 mmol), EDC (120 mg, 0.63 mmol), DMAP (76 mg, 0.63 mmol), 3-chlorobenzenesulfonamide (120 mg, 0.63 mmol) and CH_2Cl_2 (10 mL). After 24 h, the resulting residue was purified by flash chromatography (CH_2Cl_2/MeOH, 50:1) to give **4f** (104.8 mg, 0.21 mmol, 34% yield) as a white solid; mp 198–200°C; ^{1}H NMR (500 MHz, MeOD): δ 7.81 (t, *J* = 1.8 Hz, 1H), 7.76–7.75 (m, 1H), 7.50–7.47 (m, 3H), 7.42–7.41 (m, 2H), 7.37–7.32 (m, 4H), 7.26 (dd, *J* = 2.0 Hz, *J* = 8.7 Hz, 1H), 5.59 (s, 1H) ppm; ^{13}C NMR (125 MHz, MeOD): δ 173.6, 167.1, 151.6, 144.7, 143.9, 136.3, 135.4, 133.4, 131.2, 131.1, 130.0, 129.9, 129.7, 128.1, 126.6, 125.5, 119.3, 112.0, 58.2 ppm; HRMS (ESI) *m/z*: $[M+Na]^+$ Calcd for $C_{21}H_{14}Cl_2N_2NaO_4S_2$ 514.9664; found 514.9661.

2-[(5-Chlorobenzo[d]oxazol-2-yl)thio]-*N*-[(4-chlorophenyl)sulfonyl]-2-phenylacetamide (**4g**): Compound **4g** was prepared following the general procedure from 2-[(5-chlorobenzo[*d*]oxazol-2-yl)thio]-2-phenylacetic acid **2b** (200 mg, 0.63 mmol), EDC (120 mg, 0.63 mmol), DMAP (76 mg, 0.63 mmol), 4-chlorobenzenesulfonamide (120 mg, 0.63 mmol), and CH_2Cl_2 dry (10 mL). After 24 h, the resulting residue was purified by flash chromatography (CH_2Cl_2/MeOH, 50:1) to give **4g** (113 mg, 0.23 mmol, 37% yield) as a white solid; mp 179–181°C; ^{1}H NMR (500 MHz, MeOD): δ 7.88 (d, *J* = 8.7 Hz, 2H), 7.47–7.45 (m, 2H), 7.42–7.40 (m, 4H), 7.38–7.35 (m, 3H), 7.28 (dd, *J* = 2.1 Hz, *J* = 8.7 Hz, 1H), 5.60 (s, 1H) ppm; ^{13}C NMR (125 MHz, MeOD): δ 171.1, 166.5, 151.7, 143.8, 140.5, 140.1, 134.8, 131.2, 130.5, 130.3, 130.2, 129.9, 129.7, 125.6, 119.3, 112.0, 57.0 ppm; HRMS (ESI) *m/z*: $[M+Na]^+$ Calcd for $C_{21}H_{14}Cl_2N_2NaO_4S_2$ 514.9664; found 514.9664.

4.2 | Biological assays

4.2.1 | PPAR assay

EndoFectin™ transfection reagent was purchased from GeneCopoeia; all reference compounds, cell culture medium, and other

reagents were purchased from Sigma-Aldrich. Expression vectors for the chimeric receptor Gal4-DBD/hPPARα- or hPPARγ-LBD, and pGal5TKpGL3, the reporter plasmids for these chimeric receptors, were previously described.[19] The human hepatoblastoma cell line HepG2 (Interlab Cell Line Collection) was cultured in minimum essential medium (MEM) containing 10% heat-inactivated fetal bovine serum, 100 U/mL of penicillin G, and 100 µg/mL of streptomycin sulfate at 37°C and 5% CO_2. For transactivation assays, cells were seeded in a 96-well plate at a concentration of 10^4 cells per well and were transfected after 24 h with EndoFectin™, according to the manufacturer's guidelines. At 4 h posttransfection, cells were exposed to specific ligands in triplicate for a duration of 20 h. Subsequently, the cells were lysed, and their cell extracts were analyzed to quantify luciferase activity (via luminometry) and β-galactosidase activity (as normalization control). This analysis was performed using a multilabel plate reader (VICTOR^3 V, PerkinElmer), following a previously described method.[31] All transfection experiments were conducted at least twice.

4.2.2 | Cell culture

A panel of solid tumor cell lines with different expression rate of PPARs (Supporting Information S1: Table S1) was used in the in vitro study: Capan-2 (human pancreas carcinoma), SKBR3, MDA-MB-231, MCF7 (breast adenocarcinomas), HT29, HCT116, SW620 (colorectal adenocarcinomas) and A549 (lung carcinoma) were obtained from the American Type Culture Collection (ATCC) with short tandem repeat-based authentication and mycoplasma-free status. Cytotoxic selectivity was evaluated using a nontumor culture of HDF (Lonza, CC-2511). Cells were grown in RPMI-1640/DMEM medium (Gibco, Invitrogen) supplied with 10% fetal bovine serum (FBS) (Gibco, Invitrogen), 1% penicillin/streptomycin and incubated at 37°C with 5% CO_2.

4.2.3 | Cell growth/proliferation assay

The cells were seeded in a 96-well sterile plate ($3–5 \times 10^3$ cells/well) and kept overnight at 37°C in 95% humidity supplied with 5% CO_2. Series of different concentrations of compounds were made with dimethyl sulfoxide (DMSO) and serum-free medium and added to the cells. The maximum concentration of DMSO in the investigations was <1.5% and demonstrated no cell lethality. The cells were co-incubated with the compounds for 72 h. Next, 20 µL of the MTT staining reagent (5 mg/mL in phosphate cradle arrangement) was added to each well and the plates were incubated at 37°C for an additional. After 4 h incubation, the supernatant was removed and 200 µL of DMSO was added to each well to solubilize the formazan crystals, and absorbance was recorded with a 540 nm using microplate reader (Multiscan FC, Thermo Fisher Scientific).

4.2.4 | Cell-cycle distribution and apoptosis assays

The HT29 and HCT116 cells were seeded in 12-well plates at density 0.05×10^6 cells/well and 0.05×10^6 cells/well, respectively, and incubated overnight at 37°C in 95% humidity supplied with 5% CO_2 atmosphere, thereafter **3f** in three different concentrations (corresponding to its IC_{50}, ½ IC_{50} and ¼ IC_{50}) was added to the cells. The cells were co-incubated with the compound for 72 h. More than 2000 cells were analyzed in every sample using Muse® Cell Analyzer and Muse® Detection Kits (EMD Millipore Corporation) in duplicate. The Muse® Caspase 3/7 Kit (MCH100108) and Muse® Cell Cycle Kit (MCH100106) were used according to the manufacturer's instructions.

4.2.5 | Data analysis

All experiments were carried out in triplicate. The IC_{50} values were calculated by a nonlinear regression curve using GraphPad Prism version 9.0 for Windows. Data of IC_{50} are presented as mean ± standard deviation (SD).

Statistical analysis of cell cycle and apoptosis studies were performed using SPSS V. 22.0 by comparing the treatment groups to the control. Analysis of the data was performed using one-way analysis of variance (ANOVA) followed by Dunnett's test. Data are expressed as mean ± standard deviation (SD). In all cases, $p < 0.05$ was considered as statistically significant.

4.3 | Computational chemistry

4.3.1 | Protein and ligand preparation

The crystal structures of PPARα in complex with the antagonist GW6471 (PDB ID: 1KKQ)[27] and PPARγ in complex with the antagonist SR11023[28] were used in this study.

These structures were prepared for subsequent docking calculations by means of the Protein Preparation Wizard in Maestro (Protein Preparation Wizard; Epik, Schrödinger, LLC, 2023; Impact, Schrödinger, LLC; Prime, Schrödinger, LLC, 2023). Solvent molecules and other chemical components were removed, hydrogen atoms were added, bond orders, charges and atom types were adjusted. The H-bond network was optimized by performing an exhaustive sampling of rotamers, tautomers and protonation states of titratable amino acids at neutral pH. A restrained minimization of the hydrogen atoms was performed on the protein structures using the Impref module with the OPLS4 force field, by imposing a 0.3 Å RMSD limit from the initial coordinates as constraint.

The synthesized compounds **3a–h** and **4a–g** were built with Maestro 2D-sketcher and then prepared with LigPrep (LigPrep, Schrödinger, LLC, 2023) to generate suitable three-dimensional (3D) conformations and tautomerization states at pH 7.0. The compounds were then energetically minimized using the OPLS4 force field, and the resulting 3D structures were used to specify chiral centers.

4.3.2 | Docking calculations

Docking of compounds under study was performed with the Glide algorithm.[25,26] For the docking grid generation, a cubic box (10 Å × 10 Å × 10 Å in the case of PPARα, 15 Å × 15 Å × 15 Å in the case of PPARγ) surrounding each co-crystallized ligand was considered. A scaling factor of 0.8 was set for van der Waals radii of receptor atoms. Ligand sampling was allowed to be flexible. Default docking parameters were used, and no constraints were included. The Glide Score and function were used to score and rank the predicted binding poses. The optimal settings for calculations and the validity of the docking protocol were assessed by re-docking the co-crystallized ligands into their respective receptors, namely GW6471 for PPARα and SR11023 for PPARγ. The docking results revealed a very similar accommodation of the docked poses for the above-mentioned compounds with respect to the experimental binding modes (RMSD values less than 2 Å). The final binding poses were selected based on the scoring (i.e., the top-scoring enantiomer was considered as the favored configuration), the similarity to the co-crystallized ligands binding mode and the consistency of protein–ligand interactions with the experimental data.

All the figures were rendered with PyMOL (The PyMOL Molecular Graphics System, Version 2.0 Schrödinger, LLC).

ACKNOWLEDGMENTS

A.L. and F.L. acknowledge funding by the Italian Ministry of Education Progetti di Rilevante Interesse Nazionale (PRIN) grant 2022P5LPHS. A.A. acknowledges FAR funds by Ministero dell'Istruzione, dell'Università e della Ricerca. V.S.P. acknowledges funding by the RUDN University Strategic Academic Leadership Program and State Project Ministry of Science and Higher Education of Russia (agreement 075-01551-23-00; FSSF-2023-0006). C.C. acknowledges PON R&I 2014-2020 Asse IV "Istruzione e Ricerca per il recupero - REACT-EU" and Azione IV.4 "Contratti di Ricerca su tematiche dell'Innovazione". I.F., R.R., and N.M. acknowledge funding by the Ministerio de Ciencia, Innovación y Universidades (grant number PID2019-104767RB-I00) cofinanced by the European Regional Development Fund (ERDF) from FEDER, and gratefully thank CITIUS for NMR facilities. N.M. thanks the Ministerio de Ciencia, Innovación y Universidades for the Ph. D. grant.

DATA AVAILABILITY STATEMENT

The data that support the findings of this study are available from the corresponding author upon reasonable request.

ORCID

Barbara De Filippis http://orcid.org/0009-0001-1144-4614
Alessandra Ammazzalorso http://orcid.org/0000-0003-4369-1772

REFERENCES

[1] Q. Gou, X. Gong, J. Jin, J. Shi, Y. Hou, *Oncotarget* **2017**, *8*, 60704. https://doi.org/10.18632/oncotarget.19610
[2] A. Z. Mirza, I. I. Althagafi, H. Shamshad, *Eur. J. Med. Chem.* **2019**, *166*, 502. https://doi.org/10.1016/j.ejmech.2019.01.067
[3] T. Li, Q. Zhang, J. Zhang, G. Yang, Z. Shao, J. Luo, M. Fan, C. Ni, Z. Wu, X. Hu, *BMC Cancer* **2014**, *14*, 96. https://doi.org/10.1186/1471-2407-14-96
[4] M. Grabacka, K. Reiss, *PPAR. Res.* **2008**, *2008*, 1. https://doi.org/10.1155/2008/930705
[5] M. Grabacka, M. Pierzchalska, K. Reiss, *Curr. Pharm. Biotechnol.* **2013**, *14*, 342. https://doi.org/10.2174/1389201011314030009
[6] H. S. Cheng, Y. S. Yip, E. K. Y. Lim, W. Wahli, N. S. Tan, *Cancers* **2021**, *13*, 2153. https://doi.org/10.3390/cancers13092153
[7] Y. Tan, M. Wang, K. Yang, T. Chi, Z. Liao, P. Wei, *Front. Oncol.* **2021**, *11*, 599995. https://doi.org/10.3389/fonc.2021.599995
[8] A. Ammazzalorso, I. Bruno, R. Florio, L. De Lellis, A. Laghezza, C. Cerchia, B. De Filippis, M. Fantacuzzi, L. Giampietro, C. Maccallini, P. Tortorella, S. Veschi, F. Loiodice, A. Lavecchia, A. Cama, R. Amoroso, *ACS Med. Chem. Lett.* **2020**, *11*, 624. https://doi.org/10.1021/acsmedchemlett.9b00666
[9] M. Gallorini, V. Di Valerio, I. Bruno, S. Carradori, R. Amoroso, A. Cataldi, A. Ammazzalorso, *Int. J. Mol. Sci.* **2023**, *24*, 1316. https://doi.org/10.3390/ijms24021316
[10] M. J. Nanjan, M. Mohammed, B. R. Prashantha Kumar, M. J. N. Chandrasekar, *Bioorg. Chem.* **2018**, *77*, 548. https://doi.org/10.1016/j.bioorg.2018.02.009
[11] S. Wang, E. J. Dougherty, R. L. Danner, *Pharmacol. Res.* **2016**, *111*, 76. https://doi.org/10.1016/j.phrs.2016.02.028
[12] H. S. Cheng, W. R. Tan, Z. S. Low, C. Marvalim, J. Y. H. Lee, N. S. Tan, *Int. J. Mol. Sci.* **2019**, *20*, 5055. https://doi.org/10.3390/ijms20205055
[13] M. Hernandez-Quiles, M. F. Broekema, E. Kalkhoven, *Front. Endocrinol.* **2021**, *12*, 624112. https://doi.org/10.3389/fendo.2021.624112
[14] J. M. Peters, Y. M. Shah, F. J. Gonzalez, *Nat. Rev. Cancer* **2012**, *12*, 181. https://doi.org/10.1038/nrc3214
[15] T. Chi, M. Wang, X. Wang, K. Yang, F. Xie, Z. Liao, P. Wei, *Front. Oncol.* **2021**, *11*, 737776. https://doi.org/10.3389/fonc.2021.737776
[16] A. Ammazzalorso, L. De Lellis, R. Florio, A. Laghezza, B. De Filippis, M. Fantacuzzi, L. Giampietro, C. Maccallini, P. Tortorella, S. Veschi, F. Loiodice, A. Cama, R. Amoroso, *Bioorg. Med. Chem. Lett.* **2019**, *29*, 2302. https://doi.org/10.1016/j.bmcl.2019.06.020
[17] R. Amoroso, L. De Lellis, R. Florio, N. Moreno, M. Agamennone, B. De Filippis, L. Giampietro, C. Maccallini, I. Fernández, R. Recio, A. Cama, M. Fantacuzzi, A. Ammazzalorso, *Pharmaceuticals* **2022**, *15*, 937. https://doi.org/10.3390/ph15080937
[18] A. Ammazzalorso, A. Carrieri, F. Verginelli, I. Bruno, G. Carbonara, A. D'Angelo, B. De Filippis, M. Fantacuzzi, R. Florio, G. Fracchiolla, L. Giampietro, A. Giancristofaro, C. Maccallini, A. Cama, R. Amoroso, *Eur. J. Med. Chem.* **2016**, *114*, 191. https://doi.org/10.1016/j.ejmech.2016.02.064
[19] B. De Filippis, P. Linciano, A. Ammazzalorso, C. Di Giovanni, M. Fantacuzzi, L. Giampietro, A. Laghezza, C. Maccallini, P. Tortorella, A. Lavecchia, F. Loiodice, R. Amoroso, *Eur. J. Med. Chem.* **2015**, *89*, 817. https://doi.org/10.1016/j.ejmech.2014.10.083
[20] K. L. Schaefer, H. Takahashi, V. M. Morales, G. Harris, S. Barton, E. Osawa, A. Nakajima, L. J. Saubermann, *Int. J. Cancer* **2007**, *120*, 702. https://doi.org/10.1002/ijc.22361
[21] O. Abu Aboud, H. I. Wettersten, R. H. Weiss, *PLoS One* **2013**, *8*, e71115. https://doi.org/10.1371/journal.pone.0071115
[22] M. S. Lin, W. C. Chen, X. Bai, Y. D. Wang, *J. Dig. Dis.* **2007**, *8*, 82. https://doi.org/10.1111/j.1443-9573.2007.00290.x
[23] L. Sabatino, P. Ziccardi, C. Cerchia, L. Muccillo, L. Piemontese, F. Loiodice, V. Colantuoni, A. Lupo, A. Lavecchia, *Sci. Rep.* **2019**, *9*, 5434. https://doi.org/10.1038/s41598-019-41765-2
[24] J. Sun, L. Yu, X. Qu, T. Huang, *Front. Pharmacol.* **2023**, *14*, 1184794. https://doi.org/10.3389/fphar.2023.1184794

[25] R. A. Friesner, J. L. Banks, R. B. Murphy, T. A. Halgren, J. J. Klicic, D. T. Mainz, M. P. Repasky, E. H. Knoll, M. Shelley, J. K. Perry, D. E. Shaw, P. Francis, P. S. Shenkin, *J. Med. Chem*. **2004**, *47*, 1739. https://doi.org/10.1021/jm0306430

[26] T. A. Halgren, R. B. Murphy, R. A. Friesner, H. S. Beard, L. L. Frye, W. T. Pollard, J. L. Banks, *J. Med. Chem*. **2004**, *47*, 1750. https://doi.org/10.1021/jm030644s

[27] H. E. Xu, T. B. Stanley, V. G. Montana, M. H. Lambert, B. G. Shearer, J. E. Cobb, D. D. McKee, C. M. Galardi, K. D. Plunket, R. T. Nolte, D. J. Parks, J. T. Moore, S. A. Kliewer, T. M. Willson, J. B. Stimmel, *Nature* **2002**, *415*, 813. https://doi.org/10.1038/415813a

[28] R. L. Frkic, A. C. Marshall, A. L. Blayo, T. L. Pukala, T. M. Kamenecka, P. R. Griffin, J. B. Bruning, *IScience* **2018**, *5*, 69. https://doi.org/10.1016/j.isci.2018.06.012

[29] C. K. Cramer, N. Alphonse-Sullivan, S. Isom, L. J. Metheny-Barlow, T. L. Cummings, B. R. Page, D. R. Brown, A. W. Blackstock, A. M. Peiffer, R. E. Strowd, S. Rapp, G. J. Lesser, E. G. Shaw, M. D. Chan, *J. Cancer Res. Clin. Oncol*. **2019**, *145*, 337. https://doi.org/10.1007/s00432-018-2791-5

[30] T. Vogt, C. Hafner, K. Bross, F. Bataille, K. W. Jauch, A. Berand, M. Landthaler, R. Andreesen, A. Reichle, *Cancer* **2003**, *98*, 2251. https://doi.org/10.1002/cncr.11775

[31] T. Hollon, F. K. Yoshimura, *Anal. Biochem*. **1989**, *182*, 411.

SUPPORTING INFORMATION

Additional supporting information can be found online in the Supporting Information section at the end of this article.

How to cite this article: N. Moreno-Rodríguez, A. Laghezza, C. Cerchia, D. V. Sokolova, T. S. Spirina, B. De Filippis, V. Romanelli, R. Recio, I. Fernández, F. Loiodice, V. S. Pokrovsky, A. Ammazzalorso, A. Lavecchia, *Arch. Pharm*. **2024**;*357*:e2400086. https://doi.org/10.1002/ardp.202400086